Contribution of in situ acoustic emission analysis coupled with thermogravimetry to study zirconium alloy oxidation

Omar Al Haj, Véronique Peres, Eric Serris, François Grosjean, Jean Kittel, Francois Ropital, Michel Cournil

Contribution of *in situ* acoustic emission analysis coupled with thermogravimetry to study zirconium alloy oxidation

AL HAJ Omar[1], PERES Véronique[1]*, SERRIS Eric[1], GROSJEAN François[2], KITTEL Jean[2], ROPITAL François[2], COURNIL Michel[1]

[1] Ecole Nationale Supérieure des Mines, SPIN-EMSE, PRESSIC-Department, CNRS:UMR 5307, LGF, CS 62362, 42023 Saint-Etienne Cedex 02 France,
[2] IFP Energies nouvelles, Rond-point de l'échangeur de Solaize BP3, 69360 Solaize France.
* peres@emse.fr

Abstract:

Zirconium alloy (zircaloy-4) corrosion behavior under oxidizing atmosphere at high temperature was studied using thermogravimetric experiment associated with acoustic emission analysis. Under a mixture of oxygen and air in helium, an acceleration of the corrosion is observed due to the detrimental effect of nitrogen which produces zirconium nitride. The kinetic rate increases significantly after a kinetic transition (breakaway). This acceleration is accompanied by an acoustic emission activity. Most of the acoustic emission bursts were recorded after the kinetic transition or during the cooling of the sample. Acoustic emission signals analysis allows us to distinguish different populations of cracks in the ZrO_2 layer. These cracks have also been observed by SEM on *post mortem* cross section of oxidized samples and by *in-situ* microscopy observations on the top surface of the sample during oxidation.

KEYWORDS:

Thermogravimetry, Acoustic Emission, Zircaloy-4, Oxidation, High temperature corrosion

Introduction

Zirconium alloys are used as fuel cladding material in nuclear power plants. A lot of studies investigate the corrosion behavior of these alloys at high temperature under various atmospheres (air, oxygen, …) [1, 2]. During the oxidation process authors have detected a variation of the kinetic rate called breakaway. The oxidation of Zircaloy-4 is characterized by an inward ZrO_2 layer growth. Zirconia scale consists of an external monoclinic layer and of a tetragonal thin layer located close to the metal/oxide interface [3].The growth of the zirconium oxide thin film associated with a volume increase leads to residual stresses in the oxide layer. Recent works indicate the presence of different types of stresses during the oxidation of Zircaloy-4 [4, 5]. These stresses have several consequences such as cracks in the ZrO_2 layer, spallation of the thickest scales, deformation of the metal, and stabilization of the cubic crystallographic phase of zirconia [6]. Authors attribute the breakaway to the crack network in the oxide layer giving gases free access to the metal interface. The relaxation of the stresses by cracks in the oxide layer generates transient elastic waves which can be recorded and analyzed using the acoustic emission system.
Acoustic emissions correspond to abrupt variations of the stress field; elastic energy relaxation occurs and generates high frequency elastic waves (10 kHz-1200 kHz). These elastic waves caused by irreversible processes are called acoustic emission (AE) [7].
One advantage of the acoustic emission is that the frequency of the acoustic emission signals is much higher than the frequency of the environment noise (machine vibrations, human interventions …). Acoustic emission also represents an in-situ and a non-destructive method but the device needs to be adapted to the industrial environmental conditions, particularly to hot gases corrosive environments [8].

Burst analysis which is discontinuous acoustic emission analysis is preferred. Burst analysis is based on acoustic emissions related to individual events in a material. An AE burst starts when the signal amplitude exceeds the threshold (this threshold may be fixed or self-adjusting to the instrumental noise level). Several parameters can be calculated from an AE burst:

- Burst amplitude: the maximum amplitude reached during an AE Burst (dB_{AE});
- Burst duration: the time difference between the first and the last threshold crossing (µs);

- Counts: the number of threshold crossing during an AE Burst;
- Rise time: the time difference from the first threshold crossing to the Burst amplitude (µs);
- Absolute energy: integration of the square of the signal deviation from its average. Absolute energy unit is expressed in attojoules (1 aJ = 10^{-18} J);
- Average frequency: a calculated feature obtained from Count divided by Duration, which determines an average frequency over one AE Burst (kHz).

AE signals are recorded with piezoelectric sensors. These sensors convert the mechanical waves generated during the irreversible processes into electric signals. When piezoelectric sensors are placed strongly in contact with the materials, without any air voids, a low attenuation of the signal energy is observed [9, 10]. But the sensors could not be placed directly on the sample in high temperature environment. A waveguide may be used to transmit the waves from sample in the hot place to the sensors in the cold place. Alumina or platinum waveguides are mainly used [11, 12]. Alumina or platinium are characterized by a high propagation velocity. They conserve the wave forms of the AE signals with a low attenuation of the wave energy. Since 1977, some authors have associated acoustic emission with thermogravimetric analysis (TGA) to improve the knowledge of different high temperature corrosion [13,14,15,16].

We used an innovative device to perform experiments based on TGA analysis coupled with *in situ* acoustic emission. We followed high temperature oxidation of a zirconium alloy, Zircaloy-4. Simultaneous measurements of the two parameters, mass variations and AE burst, combined with *post mortem* characterization of oxidized samples, give us information which increases our level of understanding of Zircaloy-4 corrosion mechanism.

Experimental

Experiments were performed on Zircaloy-4 platelet specimens (4.8 mm x 4.6 mm x 0.5 mm). The chemical composition is given in Table 1. Samples were cleaned with acetone and ethanol before the oxidation tests.

Sn (wt %)	Fe (wt %)	O (wt %)	Cr (wt %)	C (wt ppm)	Zr
1.32 – 1.35	0.21	0.123 – 0.129	0.11	125 -140	Bal.

Table 1 Chemical composition of the Zircaloy-4 samples

Thermogravimetric analyses were carried out on a symmetric thermobalance (SETARAM TGA with Pt-Rh 6 %/ Pt-Rh 30 % thermocouples, Figure.1). The specimen's mass change was measured with a precision of ± 0.001 mg. The temperature of the oxidation test was fixed at 900 °C ± 0.1 °C; the heating rate was 15 °C/min in pure helium. Once the temperature was reached, helium was switched to a gas mixture (75 % He + 21 % O_2 + 4 % N_2). The oxidant gas was introduced by mass flow meters with a total gas flow rate of 50 ml/min for 5 hours. The cooling rate was 15 °C/min under the same process gas mixture[17].

An innovative acoustic waveguide has been developed to optimize the transmission of the acoustic signals from samples (AE source) to the sensors (Figure.1). The waveguide was conceived according to the following criteria: 1) chemical resistance against corrosive environments; 2) chemical inertness with regard to the alloy samples; 3) good transmission of the acoustic signals (low attenuation of the signal energy); 4) optimal contact with the sample. The internal diameter of the furnace (20 mm) and the maximal weight that can be supported by the balance (10 g) were taken into account. A reference with exactly the same design has been placed in the second furnace to minimize the baseline shift during experiments and to conserve the symmetric aspect between the two parts of the thermobalance. AE piezoelectric sensors were linked to the waveguide via a metallic support; sensors and metallic support were placed inside the cold part of the thermobalance where the temperature does not exceed 150 °C. The sensors are linked to an acquisition chain controlled by the AEwin™ software and data were analyzed using Noesis™ software provided by the Physical Acoustics Corporation Company. The characteristics of the acquisition chain are given in Table 2.

Instrumentation	Sensors	Threshold (dB_{AE})	System filter (KHz)	Model of the amplifier	Sampling rate	PDT - HDT - HLT
Characteristics	PICO 30	18	10 - 1200	2/4/6 gain : 60 dB_{AE}	0.25 µs (4MHz)	100 - 200 - 400 (µs)

Table 2 Main characteristics of the AE acquisition chain

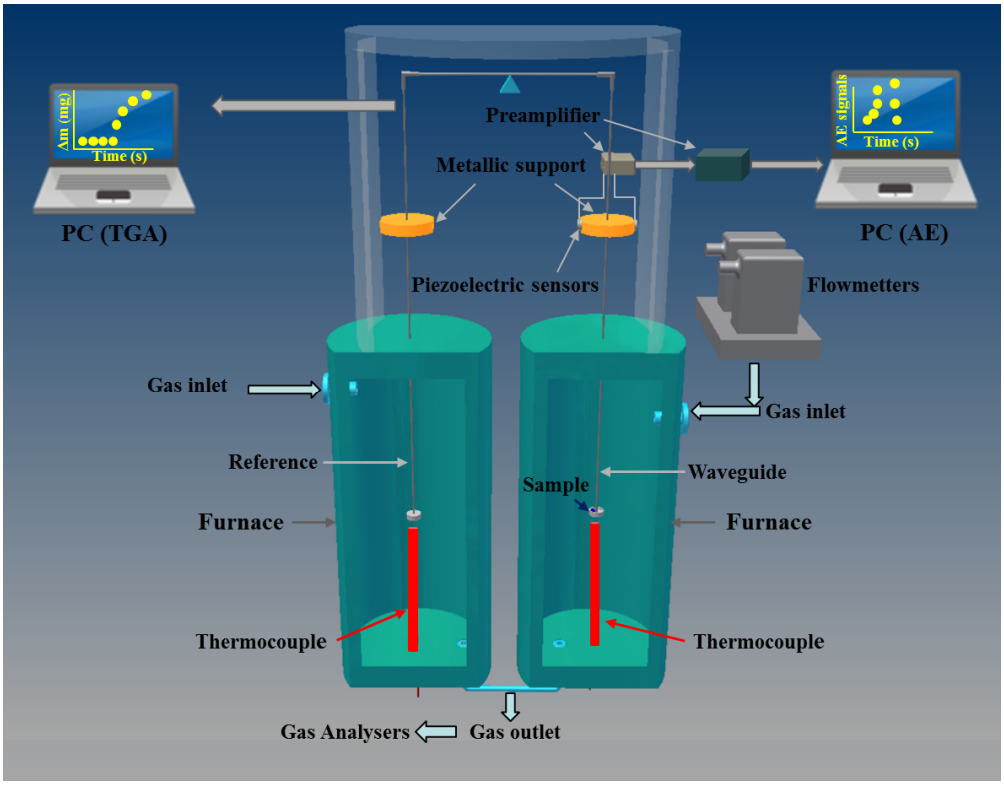

Fig. 1: Symmetric thermobalance (TGA 24) coupled with acoustic emission devices (waveguide, sensors, preamplifier)

At ambient temperature, the normalized Hsu-Nielsen test [18] was carried out to verify the AE system. This test simulates an acoustic emission event by breaking a 0.5 mm pencil lead tip against the sample surface. It generates an intense acoustic signal, similar to a natural AE source. The sensors detect a strong burst with amplitudes of at least 80 dB_{AE} for a reference voltage of 1 mV. The bursts amplitude resulting from our test amounts to 90 dB_{AE}.

Results

Thermogravimetric analysis

Blank tests without specimen were carried out to validate that the waveguide did not react with the gas mixture. The stability of the mass signal confirms the chemical inertness of the waveguide and the symmetry of the experimental device. The mass gain measurement is compatible with the AE wave guide system.

Specimen's mass variations normalized with regard to the sample surface as a function of time are presented in Figure 2 for corrosion test under (75% He + 21% O_2 + 4% N_2) named air test in the following. Rate of mass gain are presented in Figure 3.

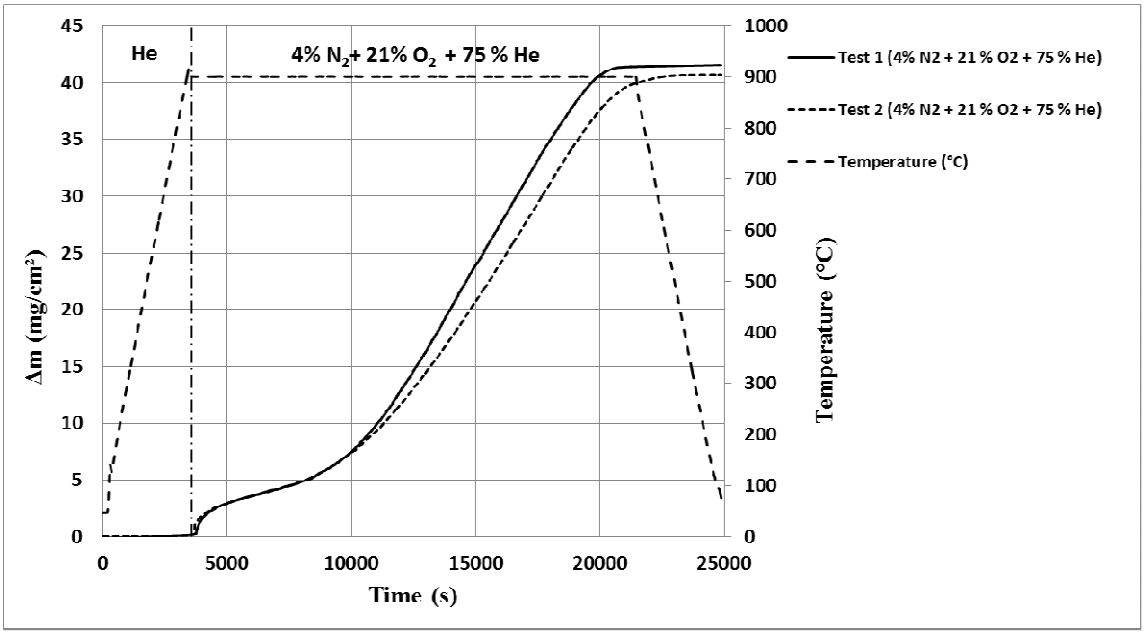

Fig. 2: Mass gain as a function of time of Zircaloy-4 oxidation tests

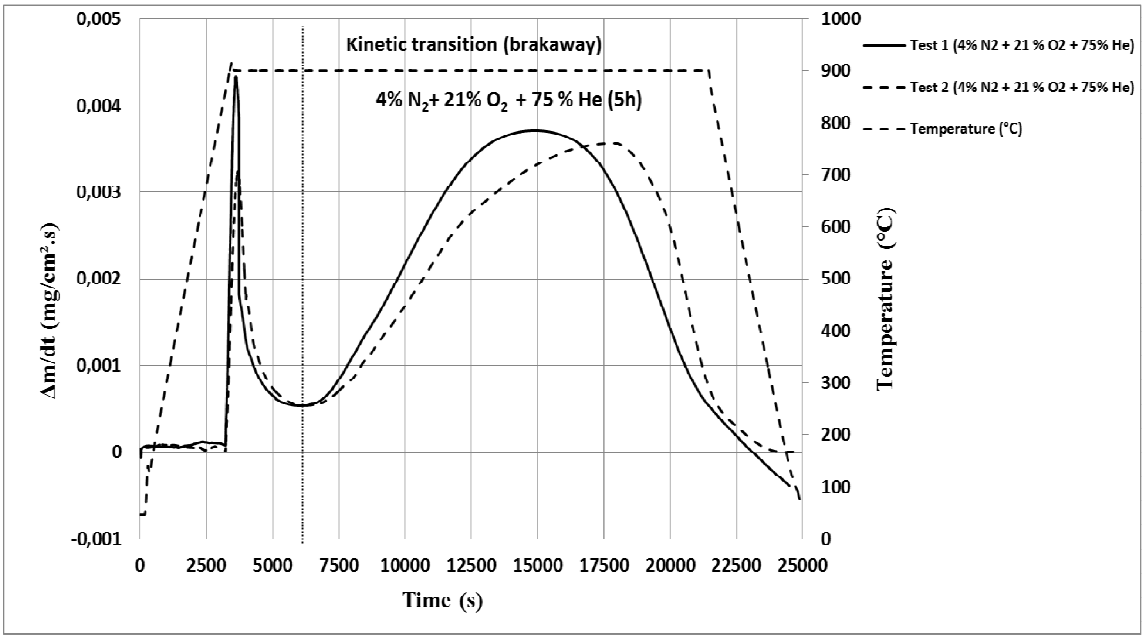

Fig. 3: Rate of mass gain as a function of time of Zircaloy-4 oxidation tests

There is no mass variation during the heating up under pure He. A significant increase of the mass during the temperature dwell time is observed, with a mass gain of 42 mg/cm² after 5 hours of oxidation. This result confirms the effect of nitrogen during the oxidation process of the Zircaloy-4 [1-2]. The reproducibility of the tests is acceptable.

An acceleration of the kinetic rate is observed after 6000 s. This acceleration corresponds to the kinetic transition. This breakaway is mainly explained by the cracking of the primary dense thin layer of ZrO_2 leading to free access of gases to the metal oxide interface. These results confirm the detrimental role of nitrogen which causes a rapid and a catastrophic oxidation of the zircaloy-4 at 900 °C.

Acoustic Emission results

Blank tests allow us to distinguish the acoustic emission signals which result from the instrumental noise. The characteristics of these AE signals are given in Table 3. These signals are short in duration with a low counts' number; 95 % of these bursts are characterized by 1 count-1 µs. The average frequency is in the range of 200 kHz to 1000 kHz (Figure 4) including the resonance frequency of the sensors (300 kHz). Burst's absolute energy is very low and doesn't exceed 0.1 aJ/burst. These bursts have been deleted from the acoustic emission signals for the rest of the study.

Bursts parameters	Amplitude (dB_{AE} / burst)	Absolute Energy (aJ/ burst)	Duration (µs/burst)	Counts number/burst	Average frequency (kHz/burst)
Blank tests	15 – 18	0 – 0.01	1 – 2	1 – 2	200 – 1000
Test 75 % He + 21 % O_2 + 4 % N_2 (Temperature dwell)	18 – 40	0.01 – 100	2 – 7 600	2 – 500	1 – 200
Test 75 % He + 21 % O_2 + 4 % N_2 (Cooling)	18 – 64	0.01 – 1 000	2 – 12 500	2 – 1 500	1 – 200

Table 3 Parameters of acoustic bursts recorded during blank and oxidation tests

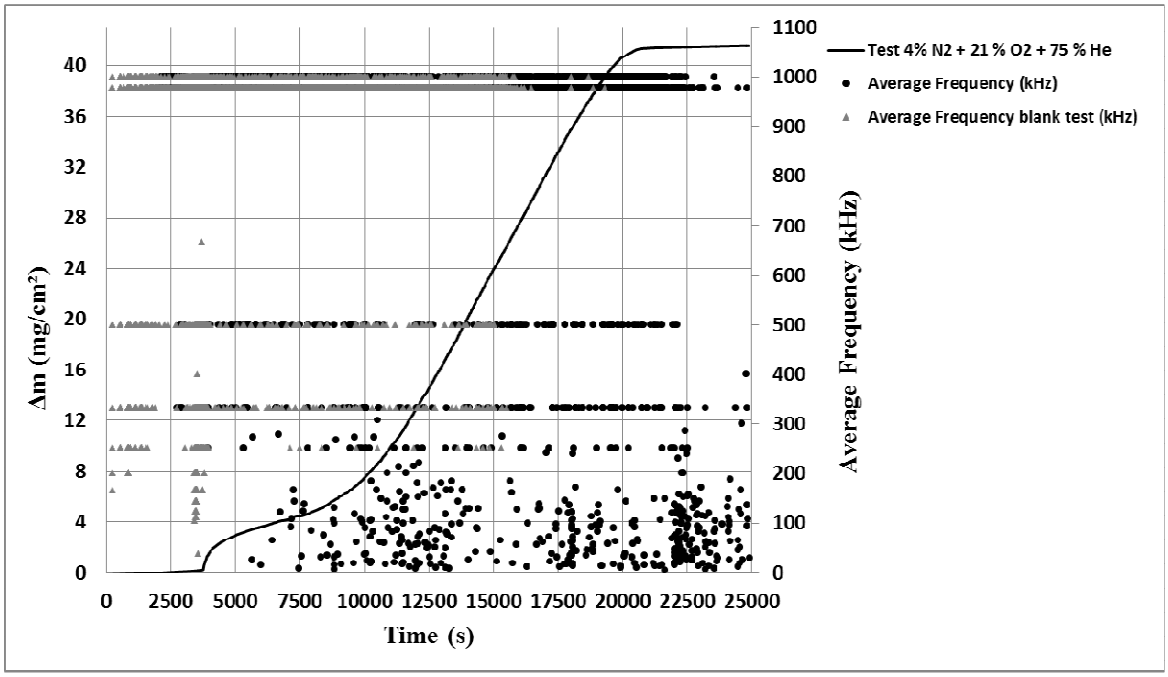

Fig. 4: Bursts average frequency variation as a function of time of a blank test (▲) and of Zircaloy-4 oxidation air test (●) and mass gain of Zircaloy-4 (–)

Figure 5 shows the bursts amplitude recorded during the corrosion tests in parallel with the kinetic rate variation as function of time. AE bursts possess a low average frequency varying between 1 kHz and 200 kHz. According to the kinetic rate curve, we note that AE bursts have been recorded just after the kinetic transition (breakaway) occurring after 6000 s. These burst are called post-transition bursts. There are also EA signals during the cooling of the sample. Post-transition bursts recorded during the temperature dwell time are characterized by mean amplitude in the range of (18 to 40) dB_{AE}. Their absolute energy average is about 10 aJ/burst. AE bursts recorded during the cooling step are more energetic (100 aJ/burst) and characterized by long duration (1000 µs/burst), and high counts number/burst (300 counts/burst as average). AE burst parameters are also detailed in Table 3.

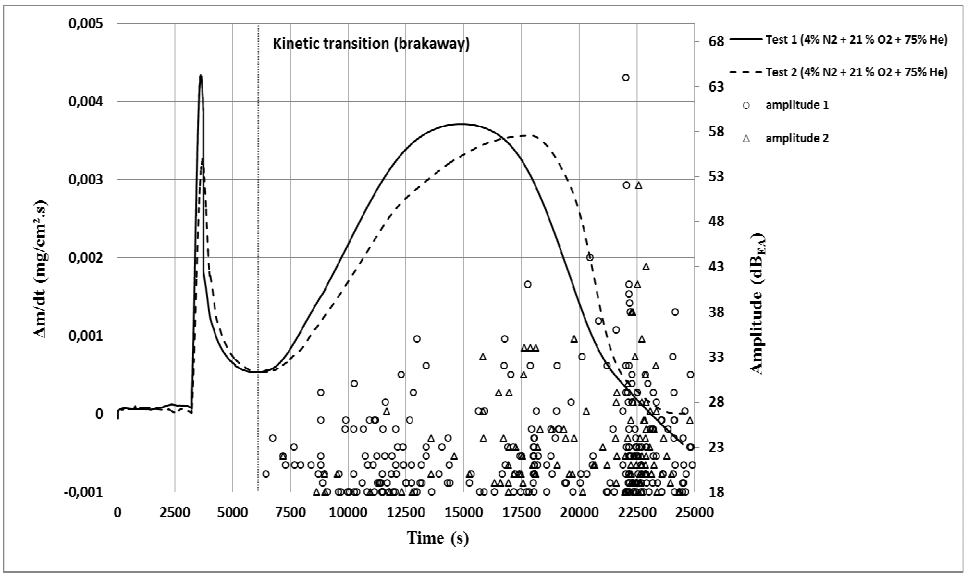

Fig. 5: Rate of mass gain and burst amplitude as a function of time during Zircaloy-4 oxidation tests

In order to confirm these results, reproducibility tests at 900°C were done (Figure 6). The reproducibility confirms that each time an important AE activity appears after the kinetic transition (post-transition bursts). One to three hundreds of bursts have been recorded during the dwell time. We can observe a maximum on the kinetic rate curve. This maximum corresponds also to a slope change of the cumulated counts curve (AE signals). Then after the maximum, the cumulated counts curves seem to be more variable.

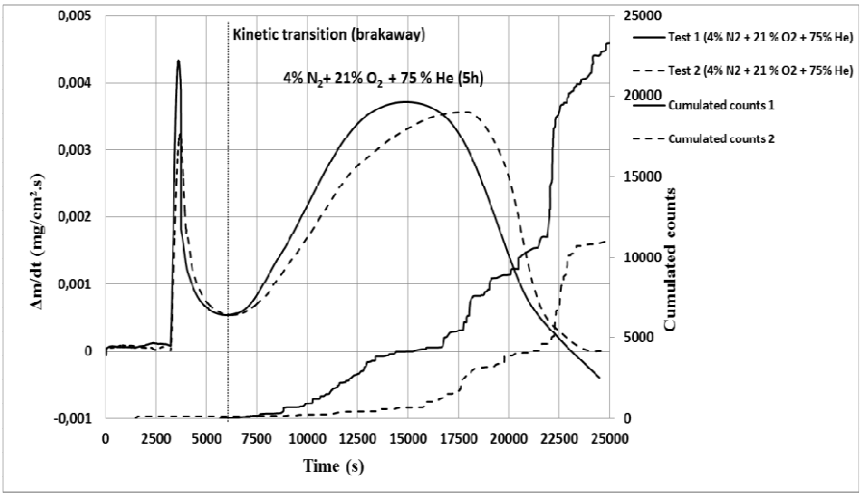

Fig. 6 Rate of mass gain as a function of time and cumulated counts number variation during the reproducibility of the Zircaloy-4 oxidation tests

The influence of the air concentration (from 0% to 5%) in the gas mixture has been demonstrated on the breakaway appearance during air oxidation tests at 900°C (Figure 7). 3% of air, meaning only 2.25% of gaseous nitrogen, is required to obtain the kinetic transition.

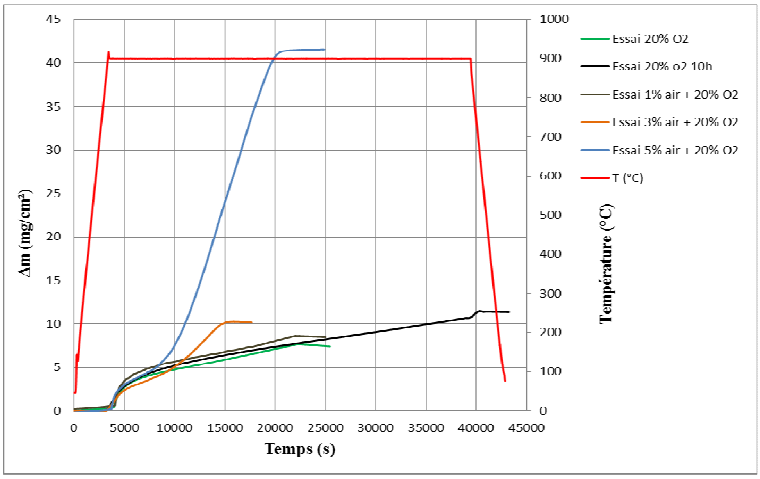

a)

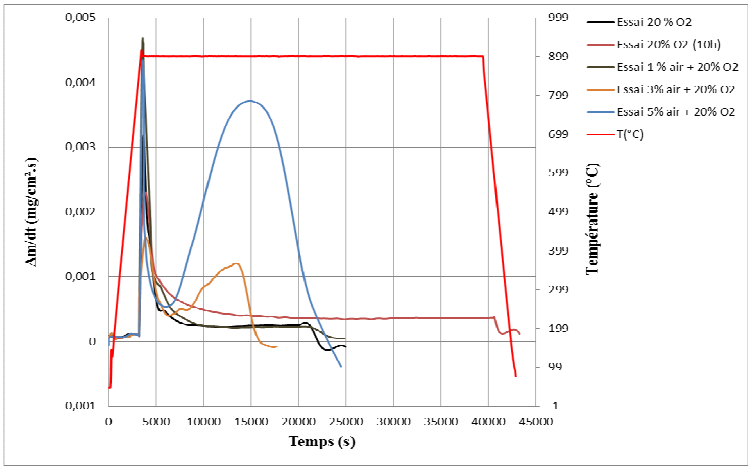

b)

Fig. 7: Mass gain (a) and rate of mass gain (b) as a function of time and air concentration of the Zircaloy-4 at 900°C

Recording of the EA signals also permits to detect the breakaway (Figure 8). Bursts appear just after the kinetic transition for test with 3% of air. No EA burst have been recorded for concentrations of air below 3%.

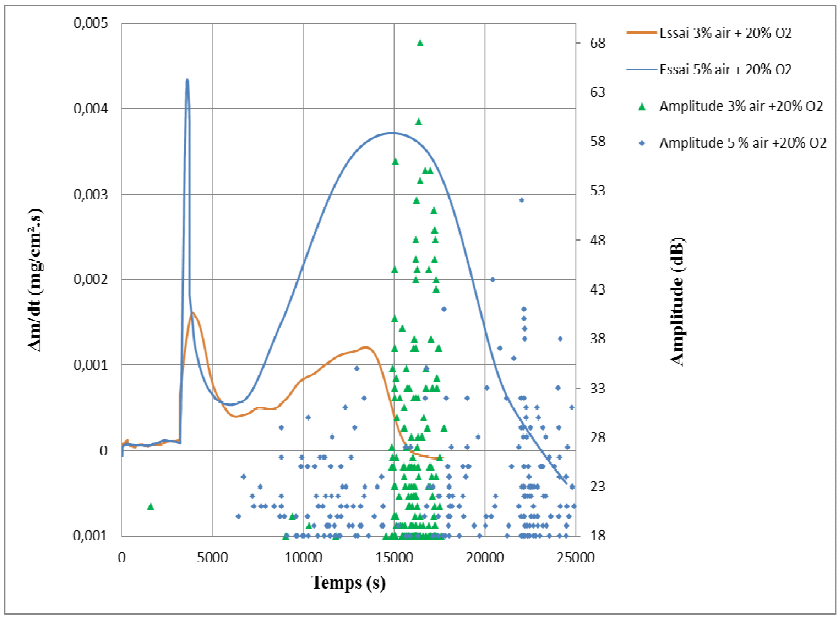

Fig. 8: Rate of mass gain and amplitude of AE burst as a function of time and air concentration of the Zircaloy-4 at 900°C

Sample characterizations

SEM cross section of oxidized sample (Figure 9) obtained with scanning electron microscopy (JEOL 6500 F) indicates that cracks are located inside the inward $Zr0_2$ layer. Cracks are visible in the external dense zirconia layer (1). They are well distributed thin, convoluted cracks, parallel to the metal oxide interface (2). Big open cracks are also periodically observed perpendicular to this interface totally crossing the zirconia layer (3). The core of the sample remains partially oxidized forming α-ZrO solid solution

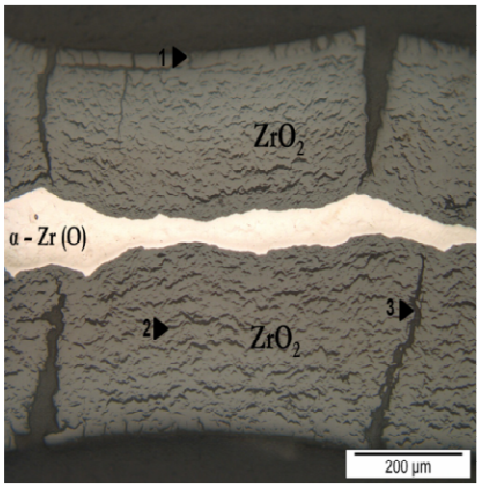

Fig. 9. SEM cross section of Zircaloy-4 oxidized at 900°C

Discussion

The oxidation of Zircaloy-4 at high temperature is still under discussion, it has been assumed that three different stages take place during the oxidation process: the pre-transition stage, the kinetic transition and post-transition stage. During the pre-transition stage the kinetic rate follows a parabolic law; the diffusion of oxygen vacancies in the protective dense zirconia layer is the limiting step. Then the kinetic rate reaches a minimum followed by an increase of rate of mass gain which corresponds to the kinetic

transition. This breakaway has been associated to the first cracks in the dense oxide layer. In our study, the kinetic transition is observed after 6000 seconds at 900°C. During the post-transition stage an important increase of the mass gain is observed; this acceleration is related to the effect of nitrogen which acts as a catalyzer during the oxidation process. ZrN is formed at the metal oxide interface. Then ZrN precipitates are oxidized with oxygen coming from the outside; nitrogen atoms are released and they are able to react with Zr metal at the internal interface creating again ZrN. Our results confirm the detrimental role of nitrogen which causes a catastrophic oxidation of the zircaloy-4 at high temperature [1-2].

According to the acoustic emission results, AE signals have been recorded during the dwell time of the oxidation test. The first acoustic signals have been recorded just after the kinetic transition.

Zirconia scale growth begins with the inward formation of a dense ZrO_2 layer at the metal-oxide interface. The Pilling and Bedworth ratio for the zirconia growth (ratio of the molar volume $V(ZrO_2)/V(Zr)$) is equal to 1.56, which means that the transformation from metal Zr to oxide ZrO_2 induces a volume dilatation. Stresses can be created in zirconia scale and in metal. The residual internal stresses increase in proportion to the zirconia scale thickness and once stresses exceed zirconia break limit, they can lead to cracks [4, 5]. Stresses are also responsible for the curvature of the metal-oxide interface.

The cracks can be associated with the AE signals recorded after the kinetic transition. The relationship between cracks and AE signals is confirmed by the *in-situ* optical microscopy observations using a RAMAN device. The cracks observed at the surface of the sample are in the scale of open cracks perpendicular to the metal oxide interface (3 in Figure 9). We can attribute some of the AE bursts to these post-transition cracks. The number of type 2 convoluted lateral cracks parallel to the metal/oxide interface surpasses the amount of AE bursts which have been recorded during the oxidation test. Even if the AE threshold is low (18 dB_{AE}), the energy of type 2 cracks seems to be too weak to generate recordable AE bursts.

Thermo-mechanical properties of Zircaloy-4 may impact the oxidation behavior of the alloy. At 900°C the β Zr phase is present and samples remain ductile; they can expand and deformed. The stresses accumulated due to the growth of a dense zirconia scale can be released by the Zircaloy-4 creep.
AE signals recorded during cooling under air correspond to energetic processes. AE bursts are characterized by an absolute energy close to 10aJ/burst in average. Figure 10 presents the evolution of the AE cumulative counts. High AE activity occurred when the temperature decreases from 750°C to 700°C. Then under air tests, AE activity remains stable during the rest of the cooling step. On the other end, for pure oxygen tests another important variation of AE activity appears for a temperature lower than 400°C.

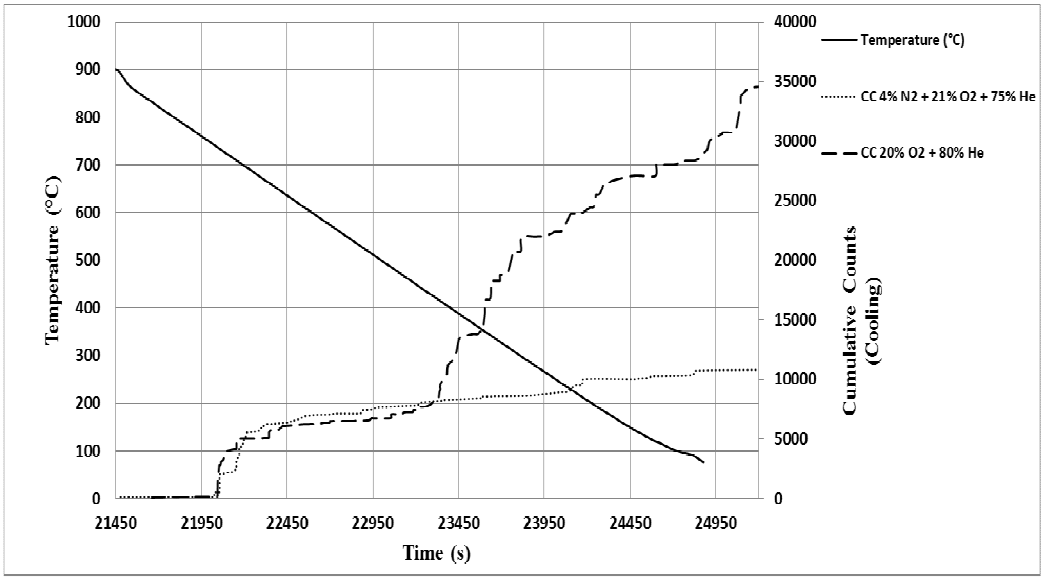

Fig. 10. Cumulated counts variation as a function of time during the cooling of the Zircaloy-4 for oxidation tests under air (---) and under oxygen 5 hours (–)

Conclusion

In situ acoustic emission analysis coupled with thermogravimetric experiments is an interesting way to improve knowledge of high temperature corrosion. AE technique allowed studying the oxidation of zircaloy-4 at 900°C. The kinetic transition was detected under air tests by a change in the rate of mass gain during the isothermal dwell time. This breakaway was also immediately detected by the AE activity. AE analysis is complementary of *post-mortem* oxidized samples characterizations. Cracks which occur during the zircaloy-4 oxidation can be distinguished from the cracks arising during cooling. The first cracks which appear after the breakaway are located in the external ZrO_2 layer perpendicular to the metal oxide interface. The AE signals correspond to these cracks. The numerous small convoluted thin cracks observed deeper in the zirconia scale are not detected by the AE technique. From these studies we can conclude that mechanisms as irreversible mechanisms, as cracks initiation and propagation, generate AE signals.

Acknowledgment

This program is a part of the FUI program IREINE (Innovation for REliability of INdustrial Equipments) dedicated to the development of devices and monitoring services to follow the corrosion of industrial process equipment, founded by the French Rhone Alpes Region.

References:

1) M. Lasserre, V. Peres, Materials and corrosion 64 (2013)
2) M. Steinbrück, M. Böttcher, Journal of Nuclear Materials 414, 276-285 (2011).
3) I. Idarraga, M. Mermoux, C. Duriez, A. Crisci, J.P. Mardon, Journal of Nuclear Materials 421,160-171 (2012).
4) M. Parise, O. Sicard , G. Cailletaud, Journal of nuclear materials 256, 35-46 (1998).
5) L. Kurpaska, J. Favergeon, L. Lahoche ; G. Moulin ; M. El-Marssi ; J-M. Roelandt, Oxidation of Metals, DOI 10.1007/s11085_012_9348_9,
6) C.C. Dollins, M. Jursich, Journal of Nuclear Materials, 113, 19-24 (1983).
7) D. Lockner, International Journal of Rock Mechanics and Mining Sciences & Geomechanics Abstracts, 30, 883–899 (1993).
8) K. Ono, Acoustic emission*, Encyclopedia of acoustics*, Wiley 1997.
9) M. Shuthe, A. Rahmel and M. Shütze, Oxidation of metals, 33-70 (1998).
10) Y. C. Zhou, T. Hashida, International Journal of Fatigue 24, 2-4, 407-417 (2002).
11) D. Renusch, M. Schütze, Surface & Coatings Technology 202, 740–744 (2007).

12) J. Sikorska, J. Pan, Journal Acoustic Emission, 22, 264-273 (2004).
13) F. Ferrer, J. Goudiakas, E. Andres and C. Brun, Journal of Acoustic emission 18, 155-160 (2000).
14) M.T. Tran, M. Boinet, A. Galerie, Y. Wouters, Corrosion Science, 52, 2365–2371 (2010).
15) R.F. Hochman Proc. of the symp. On Properties of High Temperatures Alloys with Emphasis on Environnemental Effects (Eds. Z.A. Foroulis and F.S. Pettit), the Electrochemical Society, 715 (1977).
16) HJ. Grabke, Materials and Corrosion; 49, 303-305 (1998).
17) F. Grosjean, J. Kittel, F. Ropital, E. Serris, V. Peres, Spectra Analyse 279 (2011), 35-44.
18) European standard NF EN 1330-9 (2009)-08.